

Numerical modelling of Friction Stir Processing of AlSi9Mg aluminium casting alloy

Abstract: The work presents the assumptions of a complex numerical thermo-kinetic model for Friction Stir Processing. The model makes it possible to calculate the under-tool temperature of the surface of a material being modified as well as to determine lines corresponding to the shifting of a material modified during FSP. The calculation results indicate the influence of a tool rate of rotation and of a tool travel rate on the concentration of lines and on the surface temperature. The article also reveals that a material being modified is composed of two zones in which the material is shifted, i.e. the primary and secondary zone.

Keywords: Friction Stir Processing, numerical modelling, AlSi9Mg alloy

Introduction

In order to know the processes of Friction Stir Processing (FSP) [1] or those of Friction Stir Welding (FSW) [2] it is important to determine the dependence between the process conditions and the quality and properties of joints obtained or areas modified. However, in doing so it is necessary to take into consideration a number of factors, i.e. the physical and mechanical properties of the base metal, the technological parameters of the process (rate of rotation and that of travel/welding, pressure force, tool inclination angle), the shape and type of tool, fixtures rigidity and, in some applications, the efficiency of the cooling system. In most cases the determination of the previously mentioned dependences requires only experimentation, but analytical calculations and physical simulation are also used. However, the most universal method is that of numerical simulations.

In comparison with analytical calculations, numerical methods allow the better adjustment

of data to real conditions accompanying FSW/FSP, i.e. the geometry of elements being welded, dependences of material physical properties on temperature, heat losses, and the distribution of heat sources, including friction-induced heating. The most commonly applied are Finite Element Methods and Finite Difference Methods.

The numerical simulation of FSW/FSP enables the determination of the temperature field, plasticised material motion, strain rate, joint hardness, microstructure and strain levels. Modelling requires the use of such computational systems as ANSYS, Sysweld, Forge3, STAR CCM+, ABAQUS, AcuSolve, MSC-Marc, FLUENT, FORTRAN, WELDSIM, DEFORM-3D, I-DEAS, NX, COMSOL, Matlab.

FSP modelling is carried out, among others, while adjusting and optimising the technological parameters of selective plastic forming. Paradiso et al. [3] demonstrated that the proper adjustment of forming process conditions enables, when supported by numerical modelling,

dr inż. Marek St. Węglowski (PhD Eng.) - Instytut Spawalnictwa, Testing of Materials Weldability and Welded Constructions Department; PhD Eng. Carter Hamilton - Miami University, School of Engineering and Applied Science, Oxford, Ohio, USA; Prof. Stanisław Dymek - AGH University of Science and Technology, Faculty of Metals Engineering and Industrial Computer Science

the reduction of time needed for preparing a technology as well as the reduction of manufacture costs, particularly in relation to products having complicated shapes. The tests were carried out on an AZ31 magnesium alloy. The numerical modelling made it possible to determine the places at which carrying out FSP will enable obtaining the highest plasticity and, as a result, the greatest strains during plastic working, e.g. during drawing.

Wang and Mishira [4] also carried out numerical calculations, the objective of which was to adjust proper FSP parameters so that, by means of selective superplastic forming, it would be possible to obtain the required shape of an element. The tests were carried out on a 7075 grade aluminium alloy. The calculations enabled the determination of the element thickness in the critical areas, in which, through drawing, it was necessary to obtain the required thickness of sheets.

Numerical modelling made it possible for Aljoaba et al. [5] to determine the effect of FSP conditions for AZ31B alloy on the temperature, the level of strains during the modification process, dynamic viscosity, grain size and the plasticised material travel rate. In the future the results of numerical simulation will enable the adjustment of the tool geometry and process parameters so that it will be possible to obtain the required refinement of grains in the FSP modification area.

Krumphals et al. [6] demonstrated the compatibility of the FSP physical and numerical simulations results. The numerical modelling enabled the determination of the temperature field in the test samples and of the level of strains. The results of the numerical calculations were consistent with the physical simulation carried out on the simulator of thermal-strain cycles.

Numerical modelling is also a useful instrument while analysing the motion of the plasticised material during modification. Mukherjee and Ghosh [7] used an Abaqus

system for determining the level of material strain during FSP of 5083 aluminium alloy. They also carried out the visualisation of the material motion by using 0.29 mm thick foil made of 5457 aluminium alloy.

Hsu and Hwang [8] using a DEFORM-3D system determined the field of temperature, stress and strain, as well as the travel rate of the deformed material. The tests were carried out on an AZ31 magnesium alloy. The tests results revealed that the highest temperature and the value of deformation were near the probe. A higher temperature was also observed near the upper surface of the material being modified, in the area where the dominant role was played by the shoulder and the friction phenomena taking place between the shoulder and the material surface. The results of the numerical calculations were consistent with the measurement data. It was also observed that the modified material was deformed at the highest rate near the probe.

The purpose of the tests presented in this work was to develop a complex numerical model of the modification of AlSi9Mg grade aluminium casting alloy. The model presented makes it possible to determine the field of temperature in the modification area and the motion of the plasticised material. On the basis of an overview of reference publications it is possible to state that such calculations have not been carried out until this research. The numerical calculations in the scope of the temperature field were verified through experimentation.

Test methodology

The complex thermo-kinematic model of FSW [9-11] was used to develop a model enabling the determination of temperatures in the modification area and the motion of plasticised material layers in FSP. The model was developed in the Comsol multi-physics computational environment. The details related to the design of the model itself, i.e. boundary conditions, the type of elements, simplifications in stress-strain characteristics and material physical properties

used can also be found in previous publications [9-12]. Basically, the model assumed the area of modification between the advancing and retreating sides, in which the rotary motion of the tool triggers an increase in temperature and forces the motion of the material being modified. In addition, the width of the modification area in the model is 1 mm greater than the shoulder diameter, which allowed the better illustration of the plasticised material motion around the tool.

Figure 1 presents the numerical model enabling the thermo-kinematic FSP analysis. The calculations mainly involved the use of tetrahedral finite elements. The rate of delivering the material into the tool affected area was equal to the tool travel rate v_p , and was defined in accordance with the adopted coordinate system as “+”, whereas the travel rate was defined as “-”. The boundary condition concerning the rate of material between the advancing and retreating sides and the support does not take the slide into consideration. These separation surfaces are reflected in the model grid in order to ensure the proper heat distribution compatibility across these boundaries. The boundary value related to the rate in the modification area is the following:

$$u=v_p; v=0; w=0, \quad (1)$$

where u , v and w traditionally represent the rate modules along the axes x , y and z .

Taking into consideration that fact, the experiments involved the use of the tool consisting of the shoulder only; in the model there is only one boundary condition between the tool and the material being modified – the shoulder – the material surface. In view of the foregoing, the material rate modules near the shoulder adopt the following form:

$$u=\omega y; v=-\omega x; w=0, \quad (2)$$

where ω is the FSP tool rate of rotation. The determination of the material rate field in the modification area requires knowledge of the viscosity

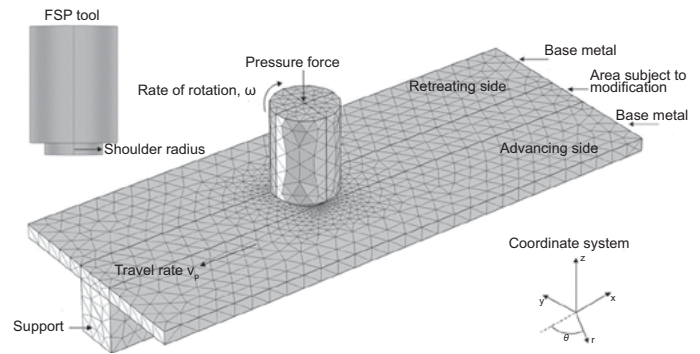


Fig. 1. Scheme of FSP numerical model

coefficient (internal friction) – μ , which is determined from the yield stress, and the rate of effective strain using the following dependence [13]:

$$\mu = \frac{\sigma_e}{3\dot{\epsilon}} \quad (3)$$

The maximum strain rate in the modification area is observed near the FSP tool, e.g.: under the shoulder or along the probe (if any), where rate gradients are the highest. The rate of strain and that of the material motion decrease considerably along with an increase of the distance to the tool. For FSW of aluminium alloys Frigaard et al. [14] determined a maximum strain rate under the shoulder of 20 s^{-1} , whilst another team [15] calculated a maximum strain rate of 100 s^{-1} under the shoulder and 30 s^{-1} 4 mm from the shoulder surface. Arora et al. [16], in the case of FSW of 2524 grade aluminium, adopted a strain rate of 9 s^{-1} . In turn, Colegrove [17] in his numerical model adopted a strain rate in the range from 0.001 to 1000 s^{-1} .

In the tests presented the calculation of the viscosity coefficient and of the yield stress were simplified by adopting the constant maximum value of the rate of effective strain at the shoulder for the whole area of modification. This assumption gives higher strain values than in reality yet enables the reliable determination of the plasticised material motion in the tool neighbourhood. Colegrove [17] demonstrated that it is the tool that plays the decisive role in heat generation and kinematic processes. For this reason, the adoption of the constant maximum strain rate triggered by the shoulder ensures good compatibility of the model with the

real conditions in the whole modification area. In order to determine this value it was assumed that the rate modules “u” and “v” decrease linearly from the shoulder surface to the lower surface of the area being modified. These assumptions were proposed, among others, by Heurtier et al. [18]. In such case the module “w” remains constant. Using the above assumptions the modules of rate in the modification area can be written as follows:

$$\begin{aligned} u &= \omega y \left(\frac{Z}{h} \right) - v_p \\ v &= -\omega x \left(\frac{Z}{h} \right) \end{aligned} \quad (4)$$

$$w=0$$

where h – depth of the layer modified.

Nandan et al. [15] suggested an extended dependence for the rate of effective strain as the function of rate gradients. Taking into consideration the above assumptions, the rate of strain can be determined using the following dependence:

$$\dot{\varepsilon} = \sqrt{\frac{1}{3} \left(\left(\frac{\partial u}{\partial z} \right)^2 + \left(\frac{\partial v}{\partial z} \right)^2 \right)} = \frac{\omega}{h} \sqrt{\frac{1}{3} (y^2 + x^2)} \quad (5)$$

The determination of x and y in equation 5 for the shoulder having radius r_w makes it possible to determine the maximum rate of effective strain from the equation below:

$$\dot{\varepsilon} = \frac{r_w \omega \sqrt{6}}{3h} \quad (6)$$

For the modification process conditions used during the tests (the depth of the layer modified in the range from 0.3 mm to 1,3 mm [19]) the rate of effective strain amounts to between 16.0 s⁻¹ and 256 s⁻¹. The calculation results are comparable with those obtained by other authors [15, 16]. Sheppard and Wright [20] proposed a dependence enabling the determination of yield stress:

$$\sigma_e = \frac{1}{\alpha} \sinh^{-1} \left[\left(\frac{Z}{A} \right)^{\frac{1}{n}} \right] \quad (7)$$

where

A, α, n – material constants; values are presented in Table 1,

Z – Zener–Hollomon parameter assuming the effect of temperature on the rate of effective strain:

$$Z = \dot{\varepsilon} \exp \left(\frac{Q}{RT} \right) \quad (8)$$

where

Q – energy of high-temperature strain activation,

R – universal gas constant,

T – temperature,

The value of material constants adopted for calculations are presented in Table 1.

Table 1. Values of materials constants adopted for calculations

Parameter	Designation	Value
Energy of high-temperature strain activation	Q	134158.4 J·mol ⁻¹
Universal gas constant	R	8.314·10 ³ J/kmol·K
Material constants	A	1.26·10 ⁸ s ⁻¹
	α	0.03055 MPa ⁻¹
	n	3.24644

During the simulation the Zener–Hollomon parameter is converted depending on the temperature in the modification area. Therefore, the model proposed assumes the dependence of temperature on the rate of effective strain, yield stress and viscosity coefficient.

Properties of materials and boundary conditions for the thermal model

In the stirring area for which the numerical model is created, the flow of heat and the motion of the plasticised material are interrelated. The thermal properties of the material, such as heat conductivity – k , and specific heat – cp , are identical in the area of the advancing and retreating sides (indicated in Figure 1). The values of the these material constants for the material being modified, for the tool and the

support, depending on the temperature, are presented in Figure 2. A more detailed analysis of the thermal model for the FSW process was presented in the previous work [21]. For FSP conducted with the tool consisting of the shoulder only the equation for the heat flux adopts the following form:

$$q_{shoulder} = \frac{2}{3} \delta_E \mu P_N \omega r_w \quad (9)$$

where

δ_E – slide coefficient,

P_N – pressure exerted by the tool on the material being modified.

The model was provided with thermal insulation between the areas of direct effect of the tool in which the motion of the plasticised material takes place and the areas in which the tool effect is only indirect and no motion of the material takes place, i.e. in the subareas from the advancing and retreating sides and near the support. Such an assumption ensured the continuous flow of heat in the individual areas as well as in the base metal, outside the area of the direct tool effect. Such an assumption is also important as regards modelling of the area between the tool work surface and the surface of the material being modified. On the boundaries of the centres which are exposed to the environment conditions, i.e. the side surfaces of the material being modified and the side surfaces of the tool, the thermal conductivity coefficient adopted was that of 15 W/m²K, assuming that convection was natural. The values adopted for the gripping part of the tool and the lower support were 200 W/m²K and 250 W/m²K respectively. The value adopted for the lower surface of the material being modified (in the place of the support) and for the upper surface of the support was 100 W/m²K. This value allowed for heat dissipation to the support. In the model proposed, heat dissipation caused by radiation was omitted. During the experimental tests no system for cooling the tool or the material being modified was used.

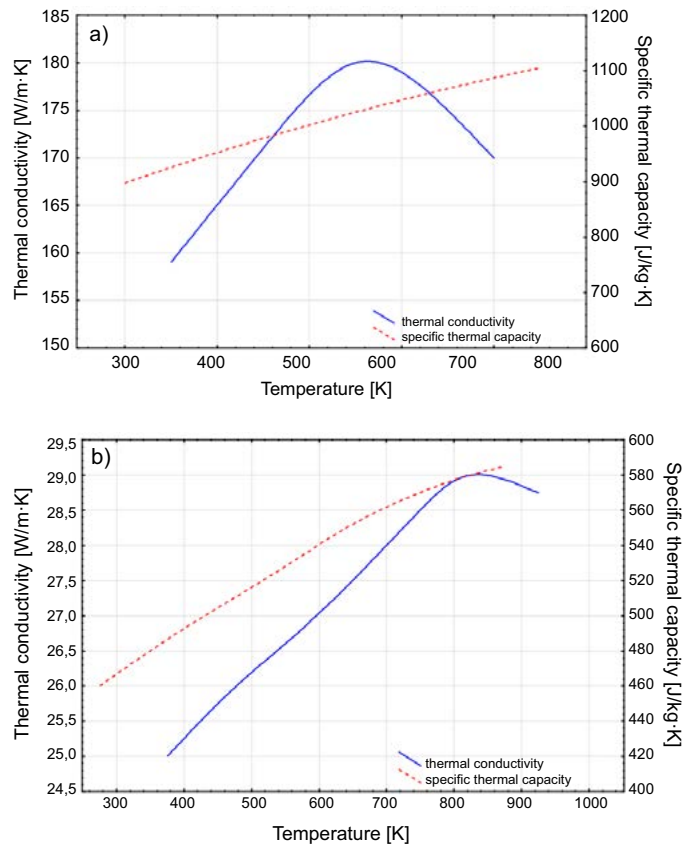


Fig. 2. Effect of temperature on thermal conductivity and specific heat, a) for aluminium alloy, b) for tool and support [9]

The research-related experimental tests were carried out on an Instytut Spawalnictwa’s FSW station consisting of an FYF32JU2 conventional milling machine, as well as the system for fixing test plates and measuring heads, i.e. a LOW-STIR head (for measuring the forces and torque acting on the tool) and a TempStir head (for measuring the tool temperature). The tests were conducted on 6mm thick test plate made of an aluminium alloy AlSi9Mg (Si - 9.0÷10.0; Fe - 0.19; Cu - 0.05; Mn - 0.10; Mg - 0.25÷0.45; Zn - 0.07; Ti - 0.15; Al - remainder), using a tool composed of a shoulder with a diameter of 20 mm, made of HS6-5-2 high-speed steel. The

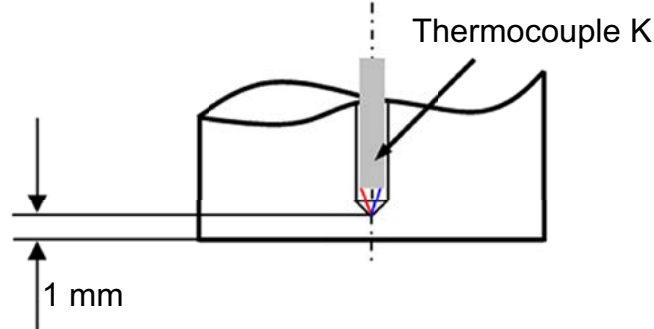


Fig. 3. Location of thermocouple in FSP tool

tests also involved the measurements of the tool temperature by means of a K-type thermocouple located in the shoulder (Fig. 3).

The tests were carried out for 5 rates of rotation, i.e. 112, 560, 900, 1400 and 1800 rev./min and 6 travel rates, i.e. 112, 224, 560, 710, 900 and 1120 mm/min. Prior to the process the tests plates were not cleaned.

Test results

Figure 4 presents the result related to the numerical modelling of the plasticised material motion in the stirring area during the modification of AlSi9Mg aluminium casting alloy ($\omega=900$ rev./min, $v_p=560$ mm/min). The FSP tool, the area in which the material motion takes place and the surface of the material undergoing the modification are presented as the contour. In turn, the lines corresponding to the motion of the plasticised material are marked in colour. The concentration of the lines implies that the motion of the material takes place mainly under the shoulder – the primary zone.

The other (secondary) zone includes the rear edge of the tool in which the material whirls behind the moving tool are generated. The friction between the shoulder surface and the material being modified cause the additional motion of the material from the advancing side towards the retreating side. This material is brought into the secondary area. Figure 4 indicates that the secondary area is also present near the rear edge of the tool. This zone is similar to eddy currents, the theory of which was developed while investigating flow phenomena in liquids. The tool rate of rotation and the tool travel rate significantly affect the shape and size of

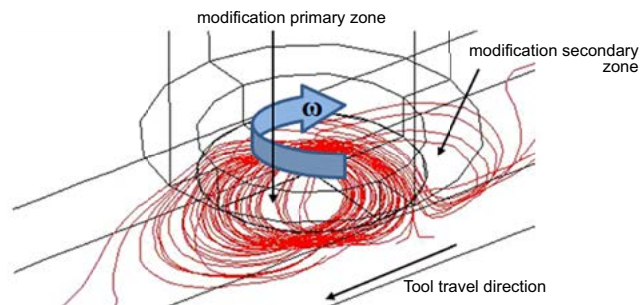


Fig. 4. Model illustrating motion of plasticised material during FSP ($\omega=900$ rev./min, $v=560$ mm/min)

individual zones. This problem will be presented in more detail further in the work.

Figure 5 presents the results related to the numerical calculations of the effect of the tool travel rate on the motion of the plasticised material at the constant tool rate of rotation amounting to $\omega=900$ rev./min. At the lowest travel rate the main area in which it possible to observe the motion of the material is concentrated near the front part of the tool, approximately in the symmetry axis. The rotary motion and the lines of material motion are visible. The secondary area is also well visible near the rear edge of the tool and includes approximately the width of the tool within the boundaries of the material being modified. An increase in the travel rate causes the main stirring zone to be clearly

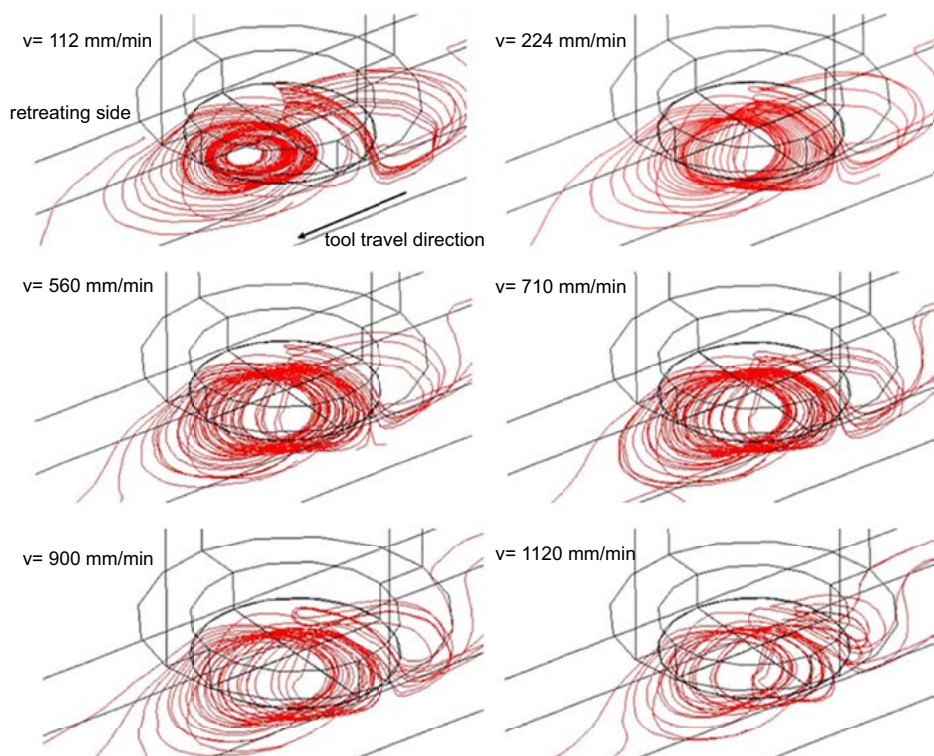


Fig. 5. Effect of tool travel rate on motion of plasticised material ($\omega=900$ rev./min)

determined. However, it should be noticed that the lines corresponding to the material motion are not only present in the axis but also move towards the rear of the tool causing the generation of additional whirls. At the same time, the diameter of the main whirl increases, indicating the lack of cohesion in the plasticised material. The secondary zone is also well visible, yet an increase in the travel rate causes a decrease of the zone.

Figure 6 presents the results related to the numerical modelling of the effect of the tool rotation rate on the motion of the plasticised material at the constant travel rate of $v=224$ mm/min. When the tool rate of rotation is low

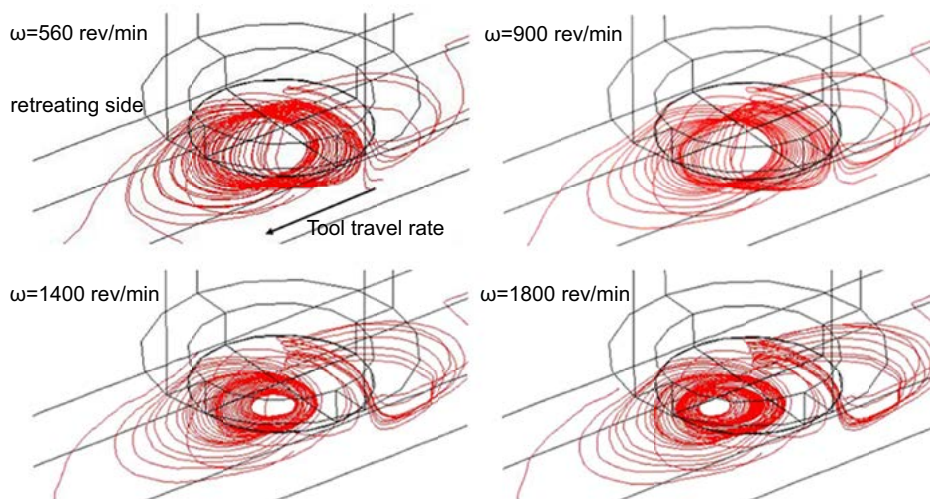


Fig. 6. Effect of tool rate of rotation on motion of plasticised material ($v=224$ mm/min)

($\omega=560$ rev./min), the primary and secondary stirring zones are well noticeable. The previously presented primary zone is in the front part of the tool but is inclined in the direction of the rear part of the tool and on the material thickness is caused by the linear motion of the tool. An increase in the tool rate of rotation decreases the diameter of the primary zone (whirl zone) and reduces the zone inclination angle. The highest rate of rotation ($\omega=1800$ rev./min) is accompanied by the strong cohesion in the rotary motion of the plasticised material and the lines corresponding to the motion of the material are concentrated in the front part of the tool, approximately to half of the tool. An increase in the tool rate of rotation is accompanied by

an increase in the concentration of the lines in the secondary zone, indicating an increase in the cohesion of the plasticised material.

The numerical calculations also included the determination of the temperature field. Figure 7 presents an exemplary profile of the numerical calculations of the temperature field on the surface of the material being modified, directly under the FSP tool ($\omega=900$ rev./min, $v_p=560$ mm/min). The temperature calculation results are provided for the material surface under the front part of the tool (PN), under the rear part of the tool (TN) as well as on the advancing side (SN) and on the retreating side (SS).

As presented in Figure 7, the highest temperature is present on the material surface under the front part of the tool. This zone is moved towards the advancing side. In turn, the area characterised by the lowest temperature is observed on the material surface under the rear part of the tool and is moved towards the retreating side. The calculation results indicate that the temperature under the front part of the tool on the advancing side is 50°C higher than in the material under the rear part of the tool on the retreating side. During FSP the base metal having a lower temperature is drawn from underneath

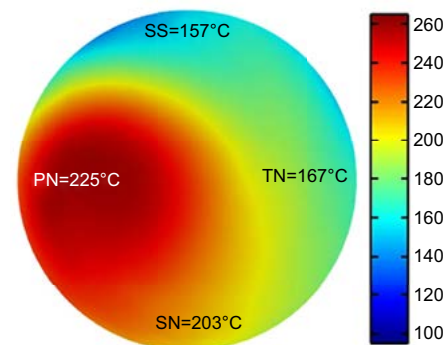


Fig. 7. Temperature distribution on modified material surface under tool during FSP ($\omega =900$ rev./min, $v_p=560$ mm/min), where PN – tool front part, TN – tool rear part, SS – retreating side, SN – advancing side

the front part of the tool and moved towards the advancing side. At the same time the modified material from beneath the rear part of the tool is also moved in the direction of the advancing side. The presented model showing the motion of the plasticised material predicts a higher temperature on the advancing rather than on the retreating side. The linear movement of the tool causes that the primary stirring zone is present under the front part of the tool (Fig. 5), which triggers an increase in the temperature. Similarly as in the case of moving of the plasticised material, the field of temperature is strongly affected by the tool rate of rotation and the tool travel rate.

Figure 8 presents the effect of the tool travel rate at the constant rate of rotation ($\omega = 900 \text{ rev./min}$) on the temperature field of the modified material surface under the tool during FSP. An increase in the travel rate causes an increase in the temperature. The zone characterised by the highest temperature is observed under the front part of the tool on the advancing side. It is possible to observe an increase in the surface temperature when the travel rate increases from 112 mm/min to 560 mm/min and 710 mm/min. At the travel rates of 560 mm/min and 710 mm/min the temperature reaches its highest value, and next decreases with a further increase of the travel rate. The numerical calculations revealed that at the rate of $v_p = 1120 \text{ mm/min}$ the surface temperature on the retreating side is lower than that observed at the rate of $v_p = 112 \text{ mm/min}$ (Fig. 8). Initially, an increase of the travel rate is accompanied by a greater generation of thermal

energy in the stirring area and by a greater volume undergoing plastic strain [19].

At greater travel rates the efficiency of heat transfer from the tool to the material being modified is reduced, among others, due to the reduced time of contact between the material undergoing plastic strain and the tool work surface as well as due to the more intense slide between the tool and the material surface. For this reason it is possible to observe a decrease in the temperature in the area under consideration.

Figure 9 presents the results of the numerical calculations of the field of the under-tool temperature of the material surface depending on the tool rate of rotation at the constant travel rate of 224 mm/min. An increase in the rate of rotation from 560 rev./min to 900 rev./min increases the temperature. Along with an increase in the rate of rotation under the constant slide conditions, the heat input caused by friction and stirring causes an increase in the temperature. A further increase in the tool rate of rotation causes the slide between the surfaces under consideration to increase and the amount of generated heat to decrease. As a result of the phenomena the surface temperature becomes

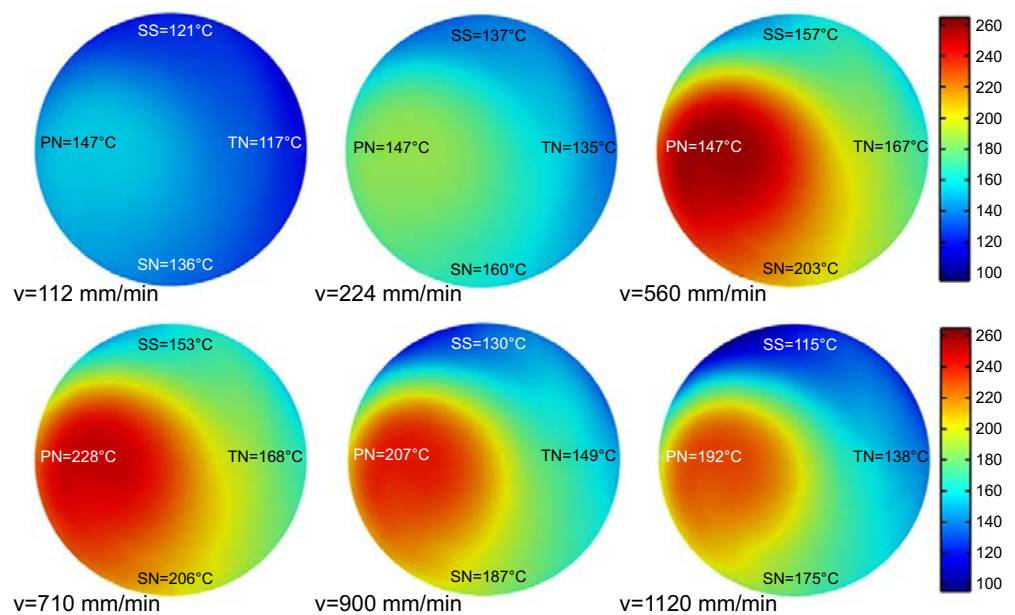


Fig. 8. Effect of tool travel rate on under-tool temperature of material surface during FSP ($\omega = 900 \text{ rev./min}$), where PN – tool front part, TN – tool rear part, SS – retreating side, SN – advancing side

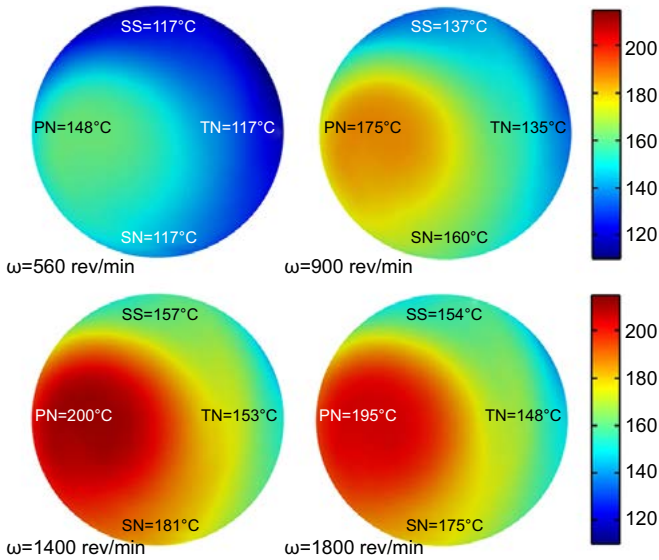


Fig. 9. Effect of tool rate of rotation on under-tool temperature of material surface during FSP ($v_p=224$ mm/min), where PN – tool front part, TN – tool rear part, SS – retreating side, SN – advancing side

stable or slightly decreased. The calculation results revealed that the highest temperature is observed for the rate of rotation amounting to 1400 rev./min and decreases when the rate of rotation increases to 1800 rev./min.

In order to verify the thermal model it was necessary to measure the temperature of the FSP tool (using a TempStir head) depending on the technological process parameters, and next, following the procedure described in the previous publication [22], calculate the temperature of the surface of the material being modified. Figure 10 presents the effect of the tool rate of rotation (at the constant travel rate of 224 mm/min) on the under-tool temperature of the surface of the material being modified. As can be seen, an increase in the rate of

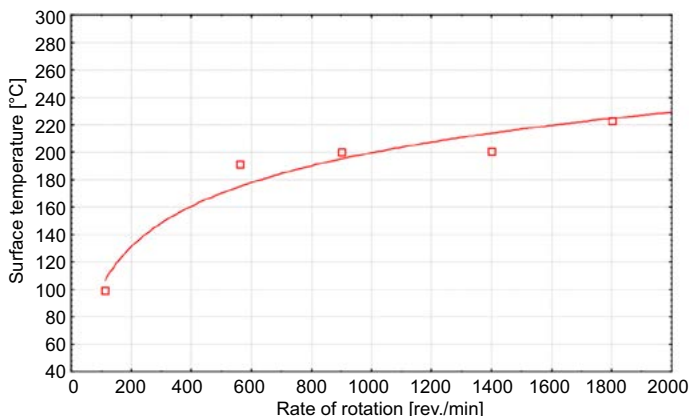


Fig. 10. Effect of tool rate of rotation on temperature of material surface under tool, $v_p=224$ mm/min

rotation causes an increase in the temperature. The differences in the quantities presented in Figures 9 and 10 result, first of all, from the fact that the temperature on the tool surface (this value is next converted) is point-measured. In addition, during the generation of the numerical model, some simplifications are adopted, e.g. the physico-chemical properties of the material being modified and the boundary conditions, which may slightly deviate from the real ones.

Summary

The work presents a complex numerical thermal-kinematic model making it possible to characterise the motion of the plasticised material during the FSP of AlSi9Mg aluminium alloy surface layers. The calculation results revealed that the primary stirring zone is formed under the front part of the tool. In the area under consideration, the tool rotation causes drawing of a portion of the base metal from the volume in front of the tool and supplying the strongly plasticised material into the area located directly under the tool. This leads to the generation of the rotary motion of the material from the surface of the plate towards its middle. Near the rear part of the tool it was possible to observe the secondary eddy-current stirring area located directly behind the moving tool. At the constant rate of rotation, an increase in the travel rate causes a decrease in the cohesion of the primary and secondary zone and the reduction of the concentration of the lines corresponding to the material motion. At the same time it was observed that at the constant travel rate an increase in the rate of rotation increases the cohesion and the concentration of these lines.

The numerical model developed helped demonstrate that the area of the highest temperature was present under the front part of the tool on the advancing side. During FSP the base metal of a significantly lower temperature is moved in portions towards the retreating side, whereas the modified material of a higher temperature is moved from the rear part of

the tool towards the advancing side causing a temperature increase in this area. At a constant rate of rotation, an increase in travel rate causes an increase in surface temperature. However, it should be noted that after exceeding a rate of 560/710 mm/min, the surface temperature decreases slightly. The dependences observed are the result of the change of friction and slide conditions between the tool work surface and the material being modified. Similarly, an increase in the tool rate of rotation, at a constant travel speed, causes an increase in temperature to the maximum value for $\omega=1400$ rev./min, followed by their stabilisation. Above the rate of $\omega=1400$ rev./min the slide between the collaborating surfaces decreases along with the amount of generated heat, and the process temperature becomes stable.

Acknowledgements:

The test results presented in this work were obtained as part of the statutory activity of Instytut Spawalnictwa in Gliwice, grant no. N507 295439 financed by the Ministry of Science and Higher Education implemented at Akademia Górniczo-Hutnicza /AGH University of Science and Technology/ in Kraków and within the confines of a bilateral project of Instytut Spawalnictwa and Miami University, the USA.

References:

1. Węglowski M.St.: Technologia Friction Stir Processing – nowe możliwości. Biuletyn Instytutu Spawalnictwa, 2011, nr 2, 25-31.
2. Pietras A., Zadroga L.: Rozwój metody zgrzewania tarcowego z mieszaniem materiału zgrzeiny (FSW) i możliwości jej zastosowania. Biuletyn Instytutu Spawalnictwa, 2003, nr 5, 148-154.
3. Paradiso V., Astarita A., Carrino L., Durante M., Franchitti S., Scherillo F., Squillace A., Velotti C.: Numerical optimization of selective superplastic forming of friction stir processed AZ31 Mg alloy. Key Engineering Materials, 2013, volumes 554-557, 2212-2220.
4. Wang Y., Mishra R.S.: Finite element simulation of selective superplastic forming of friction stir processed 7075 Al alloy. Materials Science and Engineering A, 2007, volume 463, nr 1-2, 245-248.
5. Aljoaba S.Z., Jawahir I.S., Dillon Jr O.W., Ali M.H., Khraisheh M.K.: Modelling of friction stir processing using 3D CFD analysis. International Journal of Material Forming, 2009, volume 2, 315-318.
6. Krumphals F., Gao Z., Zamani H., Mitsche S., Enzinger N., Sommitsch Ch.: Physical and numerical simulation of the microstructure evolution in AA6082 during friction stir processing by means of hot torsion and FEM. Materials Science Forum, 2013, volume 762, 590-595.
7. Mukherjee S., Ghosh A.K.: Flow visualization and estimation of strain and strain-rate during friction stir process. Materials Science and Engineering A, 2010, volume 527, nr 20, 5130-5135.
8. Hsu H.H., Hwang Y.M.: A study on friction stir process of magnesium alloy AZ31 sheet. Key Engineering Materials, 2007, volume 340-341, 1449-1454.
9. Hamilton C., Kopyściański M., Senkov O., Dymek S.: A Coupled Thermal/Material Flow Model of Friction Stir Welding Applied to Sc-Modified Aluminum Alloy. Metallurgical and Materials Transactions A, 2013, volume 44, 1730-1740.
10. Hamilton C., Dymek S., Senkov O.: Friction Stir Welding of Sc-Modified Al-Zn-Mg-Cu Alloy Extrusions. Computer Methods in Materials Science, 2009, vol. 9, 416-423.
11. Hamilton C., Dymek S., Sommers A.: A Thermal Model of Friction Stir Welding in Aluminum Alloys. International Journal of Machine Tools and Manufacture, 2008, volume 48, 1120-1130.
12. Węglowski M.St., Hamilton C.: Badanie procesu tarcowej modyfikacji warstw wierzchnich FSP. Biuletyn Instytutu Spawalnictwa, 2013, nr 1, 35-44.

13. Zienkiewicz O. C., Corneau I.C.: Visco-plasticity - Plasticity and Creep in Elastic Solids - A Unified Numerical Solution Approach. *International Journal for Numerical Methods in Engineering*, 1974, volume 8, 821-845.
14. Frigaard O., Grong O., Midling O.T.: A process model for friction stir welding of age hardening aluminum alloys. *Metallurgical and Materials Transactions A*, 2001, volume 32, 1189-1200.
15. Nandan R., Roy G.G., DebRoy T.: Numerical simulation of three-dimensional heat transfer and plastic flow during friction stir welding. *Metallurgical and Materials Transactions A*, 2006, volume 37, 1247-59.
16. Arora A., Zhang Z., De A., DebRoy T.: Strains and strain rates during friction stir welding. *Scripta Materialia*, 2009, volume 61, 863-866.
17. Colegrove P.A., Shercliff H.R., Zettler R.: Model for predicting heat generation and temperature in friction stir welding from the material properties. *Science and Technology of Welding and Joining*, 2007, volume 12, nr 4, 284-297.
18. Heurtier P., Jones M.J., Desrayaud C., Driver J.H., Montheillet F., Allehaux D.: Mechanical and thermal modelling of friction stir welding. *Journal of Materials Processing Technology*, 2006, volume 171, 348-357.
19. Węglowski M.St., Dymek S.: Microstructural modification of cast aluminium alloy AlSi9Mg via Friction Modified Processing. *Archives of Metallurgy and Materials*, 2012, volume 57, 71-78.
20. Sheppard T., Wright D.S.: Determination of flow stress: Part 1. Constitutive equation for aluminium alloys at elevated temperatures. *Metals Technology*, 1979, volume 6, 215-223.
21. Hamilton C., Sommers A., Dymek S.: A thermal model of friction stir welding applied to Sc-modified Al-Zn-Mg-Cu alloy extrusions. *International Journal of Machine Tools & Manufacture*, 2009, volume 49, 230-238.
22. Węglowski M.St., Dymek S.: Relationship between Friction Stir Processing parameters and torque, temperature and the penetration depth of the tool. *Archives of Civil and Mechanical Engineering*, 2013, volume 13, 186-191.